Available online at www.sciencedirect.com

ScienceDirect

Procedia Manufacturing 30 (2019) 373–379

Procedia MANUFACTURING

www.elsevier.com/locate/procedia

14th Global Congress on Manufacturing and Management (GCMM-2018)

Investigation of mechanical properties and morphology of hydrothermally manufactured titanium dioxide nanostructured surfaces

Alka Jaggessar[a], Tuquabo Tesfamicheal[a], Hongxia Wang[a], Cheng Yan[a] and Prasad KDV Yarlagadda[a,*]

[a]*Queensland University of Technology, 2 George Street, Brisbane 4000, Australia*

Abstract

The hydrothermal process is a commonly used technique for manufacturing nanoparticles and nanostructured surfaces, and has been used to manufacture titanium dioxide (TiO_2) nanostructured bactericidal surfaces. This work examines the mechanical properties, surface morphology and stability of the TiO_2 surface as a function of NaOH concentration. At NaOH concentrations below 1.50 M, individual pillar-like nanostructures with high Young's modulus were formed. When NaOH concentration was increased above 1.50 M, nanostructure tips fused together to form a large interconnected mesh-like network. This mesh-like structure caused a reduction in the Young's modulus and hardness of the titanium dioxide surface. The mechanical properties of the TiO_2 remained constant over a 6 month period, indicating stability of the nanostructures. This work demonstrates the synthesis of stable TiO_2 nanostructured surfaces of different Young's modulus, hardness and surface morphology using the hydrothermal method, with potential application in orthopedic implants.

Keywords: Hydrothermal Synthesis; Nanoindentation; Nanostructures; TiO_2.

* Corresponding author *E-mail address:* y.prasad@qut.edu.au

2351-9789
10.1016/j.promfg.2019.02.052

1. Introduction

In recent years there has been an increased research focus on the use of nanostructures for killing bacteria and resisting the formation of biofilms. Studies have shown that nano-textured surfaces found on cicada wings, dragonfly wings, butterfly wings, lotus leaves and shark skin are effective in killing various strains of bacteria [1-10]. Many studies have attempted to replicate these textures using various methods, artificial substrates and materials such as TiO_2, black silicon and various polymers [11-15]. The emergence of these textures as potential surfaces for orthopedic and dental implants have given rise to the question of material surface properties and mechanical stability of these structures.

The hydrothermal process is a fairly common technique for synthesizing nanostructures, involving the manipulation of precursors and recrystallization of materials under high temperature and pressure [16, 17]. Hydrothermal reaction parameters such as precursor concentration, reaction temperature and reaction duration significantly affect the resulting surface properties. Increasing precursor concentration has been found to increase the density of fabricated structures, with high concentrations forming highly dense, close packed arrays [18]. Similarly, larger particles are formed at high temperatures (approximately 180°C) and longer reaction durations [16, 19, 20].

While these studies have focused on the morphological and topographical changes to nanostructures with varying parameters, there is little known about changes in mechanical behavior due to parameter alterations. This study investigated the effect of NaOH concentration used in the hydrothermal reaction on the morphological and mechanical properties of the fabricated textured surfaces. In addition, this study also explored the mechanical stability of the fabricated surfaces to establish whether these surfaces could be suitable for long term applications.

2. Experimental Method

This section describes the experimental and characterization methods used in the study. TiO_2 nanostructured surfaces were fabricated using the hydrothermal process and characterized using X-Ray diffraction (XRD), scanning electron microscopy (SEM), and nanoindentation.

2.1. Surface Fabrication

Six nano and micro-textured TiO_2 surfaces were fabricated by varying the concentration of the NaOH precursor from 0.1 to 2.0 M. A titanium plate was cut to 10 mm x 10 mm size and polished to a 0.04 μm surface roughness. The samples were sonicated in acetone for 10 minutes and placed in a custom-made PTFE holder in a 125 mL Parr acid digestion vessel. 60 mL of NaOH solution with varying concentrations (see Table 1 for experimental concentrations) was added to the vessel. The samples were then left to react for 3 hours at 240°C before it was removed and left to cool to room temperature overnight. Once cool, each sample was washed 3 times with 18.2 MΩ distilled H_2O before being dried with N_2 gas, and placed in a furnace for 1 hour at 300°C (for annealing). The annealed samples were then submerged in 20 mL of 0.6 M HCl for 30 minutes, then rinsed thoroughly in H_2O. The samples were then placed back in the furnace for 2 hours at 600°C for calcination [19, 21]. Samples were removed from the furnace when at room temperature.

Table 1: Experimental NaOH concentrations used in the hydrothermal reaction

Sample Name (NaOH Concentration (M)_Reaction Time (Hrs)_Reaction Temperature(°C))	NaOH Concentration (M)
0.10_3_240	0.10
0.25_3_240	0.25
0.50_3_240	0.50
1.00_3_240	1.00
1.50_3_240	1.50
2.00_3_240	2.00

2.2. Surface Characterization

The surface morphology of the nanostructured TiO_2 surfaces was analyzed using a JEOL JSM-7001F SEM. Surface images were obtained at a 40° tilt angle and an accelerated voltage of 15kV. Crystal phases of the samples were examined using XRD to confirm the presence of TiO_2. The XRD testing was conducting using a Rigaku SmartLab Diffractometer (with a Cu source at 40 kV and 40 mA), operating in a parallel beam model with a Hypix 3000 detector (0D mode). A 2° incidence was used with a 2Θ scan angle. Patterns were collected over 1 hour at a step size of 0.0152°, in the angle range of 2Θ = 5 - 75°.

Mechanical properties of the surfaces were measured using a Hysitron TI 950 nanoindenter, with a Berkovich indenter tip (three-sided pyramidal tip with an approximate radius of 100 nm and included angle of 142.3° [22]). The tip area function was calibrated using fused silica, with known elastic modulus and hardness. Each sample was indented 10 times with a 10 µm spacing between each indent. The indent was performed using a trapezoid load function, with a loading rate of 40 µN/s (for 5 seconds). The samples were held at a peak load of 200 µN for 10 seconds before unloading. To test the mechanical stability of the structures over time, mechanical property measurements were repeated after 6 months and results compared to the fresh samples. Mech Test 1 denotes nanoindentation test results from initial testing, and Mech Test 2 refers to measurements taken 6 months after Test 1. Between mechanical tests, the samples were stored in petri dishes in a laboratory environment.

2.3. Statistical Analysis

Statistical analysis was performed using a two-way ANOVA Sidak's multiple comparison test to compare significant results of Mech Test 1 and Mech Test 2. Significant results are indicated in Figure 4, where *p<0.1, **p<0.01, ***p<0.001 and ****p<0.0001.

3. Results and Discussion

3.1. Surface Morphology

After fabrication, XRD was measurements were performed on one of the samples (*1.00_3_240*) to confirm the formation of TiO_2. Figure 1 shows the XRD spectrum obtained from this sample.

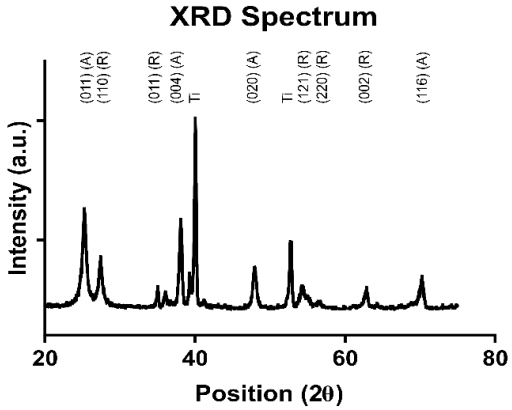

Figure 1: XRD spectrum of *1.00_3_240*

The spectrum obtained from XRD shows the presence of metallic Ti and TiO_2 with anatase and rutile phases. Diffraction peaks that appear on the XRD pattern agree well with the diffraction peak of these phases [19, 23], confirming that the nanostructures are TiO_2 on a Ti substrate.

SEM analysis shows that the overall morphology (TiO_2 structure shape and dimensions) changes with NaOH concentration. Figure 2 shows the SEM images of the various surface textures fabricated under the experimental parameters in Table 1. Figure 2 shows that fabricated structures change from short, random, pillar-like structures at low NaOH concentrations (Figure 2 (a) – (d)) to a large, interconnected mesh-like structure at high NaOH concentrations (Figure 2 (e) – (f)). This is further evidenced by the increase in structure height with increased reaction concentrations Table 2.

Figure 2: Surface morphology of surfaces fabricated at a NaOH concentration of (a) 0.10 M (b) 0.25 M (c) 0.50 M (d) 1.00 M (e) 1.50 M (f) 2.00 M

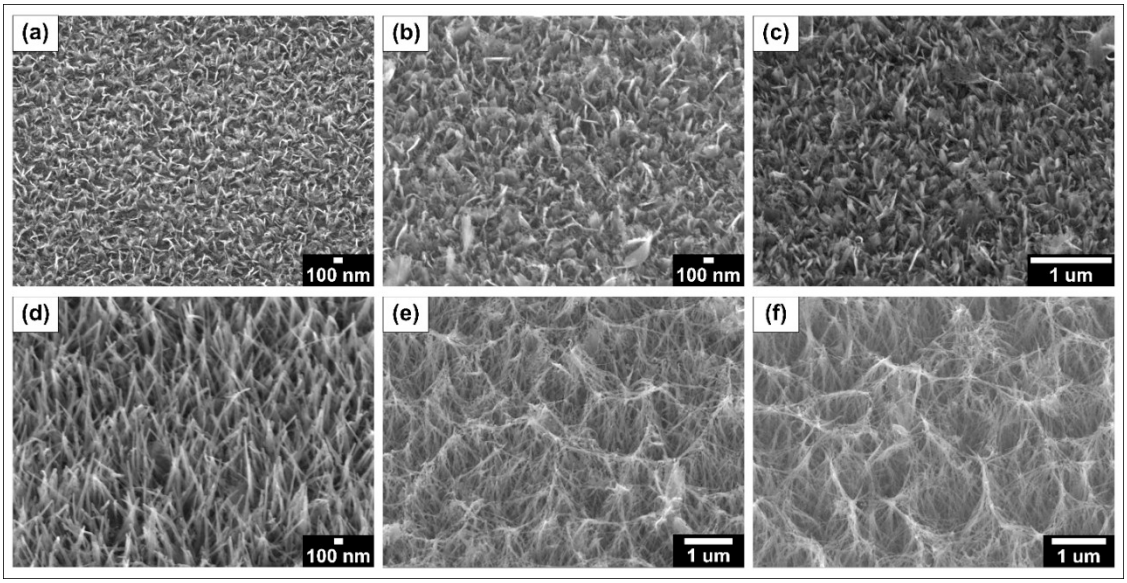

Table 2: Average structure dimensions

NaOH Concentration (M)	Average Height (nm)	Average Diameter (nm)
0.10	212.50 ± 24.58	16.70 ± 2.16
0.25	244.70 ± 21.33	27.39 ± 5.04
0.50	295.00 ± 27.15	28.70 ± 4.20
1.00	298.00 ± 33.15	55.10 ± 12.55
1.50	850.00 ± 92.30	31.43 ± 4.83
2.00	947.00 ± 254.51	38.85 ± 3.97

Figure 3 (a) shows that as NaOH concentration increases, average height of the nanorods increase. Nanostructures stay individualized at random orientation angles until NaOH concentration reaches 1.00 M. When the NaOH concentration is increased beyond 1.50 M a large interconnected web of TiO_2 structures is observed (Figure 2 (e) and (f)). Increasing NaOH concentration has caused a higher number of nucleation sites on the surface. This phenomena, coupled with the random orientation angle of structural growth, causes structures to fuse ultimately creating the large, highly connected array observed [19, 20]. This confirms that high NaOH concentrations affect the morphology and density of the fabricated surface.

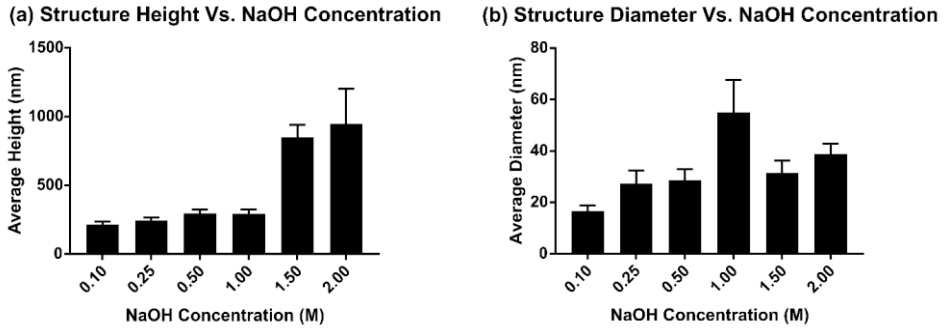

Figure 3: Average (a) height and (b) diameter of structures formed under various NaOH concentrations

3.2. Mechanical Properties and Stability

Elastic modulus and hardness of each sample were measured using nanoindention. The hardness of the sample was calculated using [22, 24]:

$$H = \frac{P_{\max}}{A_c} \tag{1}$$

Where H is the hardness of the material, P_{max} is the maximum applied load and A_c is the contact area. Elastic modulus was calculated using:

$$\frac{1}{E_r} = \frac{1-\nu_m^2}{E_m} + \frac{1-\nu_i^2}{E_i} \tag{2}$$

Where E_r is the reduced modulus, E_m and ν_m are the elastic modulus and Poisson's ratio of the sample material respectively, and E_i and ν_i are the elastic modulus and Poisson's ration of the indenter tip respectively. A standard Berkovich diamond indenter tip has an E_i = 1140 GPa and ν_i = 0.07 [24]. The ν_m of the nano-arrays were chosen to be the same as bulk TiO_2 (0.28) [22]. The average elastic moduli and hardness values of Mech Test 1 (initial test) and Mech Test 2 (6 months after initial test) are shown in Table 3:

Table 3: Mechanical properties of the fabricated surface measure 6 months apart

Sample	Mech Test 1		Mech Test 2	
	Elastic Modulus (GPa)	Hardness (MPa)	Elastic Modulus (GPa)	Hardness (MPa)
0.10_3_240	10.20 ± 1.06	1015.08 ± 160.72	8.82 ± 2.04	777.92 ± 250.33
0.25_3_240	4.11 ± 0.76	219.24 ± 69.66	3.43 ± 0.57	141.08 ± 48.98
0.50_3_240	13.89 ± 2.36	233.86 ± 46.39	11.03 ± 1.28	397.35 ± 69.12
1.00_3_240	2.73 ± 0.61	14.75 ± 1.78	2.03 ± 0.60	14.40 ± 1.37
1.50_3_240	1.88 ± 0.72	15.95 ± 2.74	1.21 ± 0.12	11.60 ± 1.83
2.00_3_240	1.10 ± 0.22	18.33 ± 3.85	1.73 ± 0.56	23.71 ± 22.71

Results in Figure 4 show that a NaOH concentration of 0.50 M (sample *0.50_3_240*) produces the stiffest structures. At this concentration, structure height is at an average of 295 nm (Table 2). This result is notable, as the samples produced at slightly lower (0.25 M) and slightly higher (1.00 M) concentrations produce structures with

significantly lower moduli. It is possible that this concentration produces surfaces with a particular structure size and orientation that are conducive to highly stiff structures. With the exception of sample *0.50_3_240*, there is a general trend of decreasing stiffness with increasing NaOH concentration, which relates to increased structure height. The data shows that in general, as nanostructure height increases, the nanostructures become less stiff giving a lower Young's modulus. This could be a result of the formation of the nanowire mesh formed at high NaOH concentrations (1.50 and 2.00 M).

The stability of the structures over time was determined by repeating the nanoindentation tests 6 months after initial testing using the same tip, parameters and load function. The results of the stability test show that on average, there is no significant change of the Young's moduli in 6 months after initial testing. This is a promising result, as it indicates that structures remain stable after an extended period of time, without significant change. While there is a statistically significant change in Young's modulus measured for sample *0.50_3_240* (Figure 4), Table 3 shows that there is a 2 GPa difference between measurements, which is relatively small given the 13.89 GPa initial measurements.

4. Conclusion

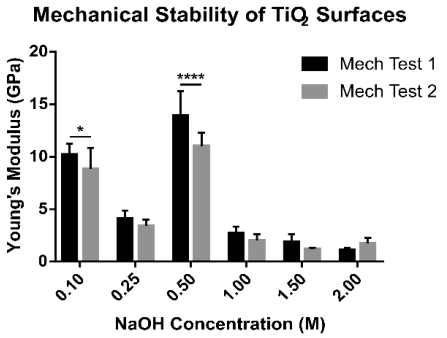

Figure 4: Mechanical stability of fabricated surfaces where * p<0.1, ** p<0.01, *** p<0.001 and **** p<0.0001

This study examined the effect of NaOH concentration on the morphology and mechanical properties of hydrothermally synthesized TiO_2 nano and micro-textured surfaces. The results show that increasing NaOH concentration strongly influences the height, shape and overall morphology of the structures. At low concentrations (up to 1.00 M) structures are individual and pillar-like in shape with random orientation angles. At higher concentrations (1.50 and 2.00 M), structures grow into an interconnected nanowire mesh array. Mechanical properties generally increase with decreasing NaOH concentration, due to the smaller dimensions and heights of the nanostructures (212.5 – 298.0 nm). Small concentrations have produced stiff structures, with Young's modulus generally decreasing with increasing NaOH concentration. The indentation test also shows that structures are generally stable over time, which is a promising result for potential orthopedic applications. The significance of this finding is that with time, structures should not lose their mechanical properties, indicating that the mechanical nature of the structures remains constant over time, widening the applicability of nano-textured surfaces for long term applications.

Acknowledgements

The authors would like to acknowledge Dotmar Engineering Plastic Products for providing PTFE, Dilini Galpayage Dona for assisting in nanoindentation testing, Donald McAuley for sample preparation, Henry Spratt for completing XRD measurements, the Central Analytical Research Facility (QUT), Design and Manufacturing Centre (QUT) and the Institute for Future Environments (QUT).

References

[1] C.D. Bandara, S. Singh, I.O. Afara, A. Wolff, T. Tesfamichael, K. Ostrikov, A. Oloyede, Bactericidal effects of natural nanotopography of dragonfly wing on Escherichia coli, ACS Applied Materials & Interfaces 9 (2017) 6746-6760.
[2] C.M. Bhadra, V.K. Truong, V.T.H. Pham, M. Al Kobaisi, G. Seniutinas, J.Y. Wang, S. Juodkazis, R.J. Crawford, E.P. Ivanova, Antibacterial titanium nano-patterned arrays inspired by dragonfly wings, Scientific Reports 5 (2015) 16817.
[3] Y.T. Cheng, D.E. Rodak, C.A. Wong, C.A. Hayden, Effects of micro- and nano-structures on the self-cleaning behaviour of lotus leaves, Nanotechnology 17 (2006) 1359-1362.
[4] Z. Guo, W. Liu, Biomimic from the superhydrophobic plant leaves in nature: Binary structure and unitary structure, Plant Science 172 (2007) 1103-1112.
[5] J. Hasan, H.K. Webb, V.K. Truong, S. Pogodin, V.A. Baulin, G.S. Watson, J.A. Watson, R.J. Crawford, E.P. Ivanova, Selective bactericidal activity of nanopatterned superhydrophobic cicada Psaltoda claripennis wing surfaces, Applied Microbiology and Biotechnology 97 (2013) 9257-9262.
[6] Y.C. Jung, B. Bhushan, Biomimetic structures for fluid drag reduction in laminar and turbulent flows, Journal of Physics: Condensed Matter 22 (2010) 035104.
[7] T.W. Kim, Assessment of hydro/oleophobicity for shark skin replica with riblets, Journal of Nanoscience and Nanotechnology 14 (2014) 7562-7568.
[8] J. Ma, Y. Sun, K. Gleichauf, J. Lou, Q. Li, Nanostructure on taro leaves resists fouling by colloids and bacteria under submerged conditions, Langmuir 27 (2011) 10035-10040.
[9] M. Ma, R.M. Hill, Superhydrophobic surfaces, Current Opinion in Colloid & Interface Science 11 (2006) 193-202.
[10] S. Pogodin, J. Hasan, V.A. Baulin, H.K. Webb, V.K. Truong, T.H. Phong Nguyen, V. Boshkovikj, C.J. Fluke, G.S. Watson, J.A. Watson, R.J. Crawford, E.P. Ivanova, Biophysical model of bacterial cell interactions with nanopatterned cicada wing surfaces, Biophysical Journal 104 (2013) 835-840.
[11] G.D. Bixler, B. Bhushan, Rice- and butterfly-wing effect inspired self-cleaning and low drag micro/nanopatterned surfaces in water, oil, and air flow, Nanoscale 6 (2013) 76-96.
[12] M.N. Dickson, E.I. Liang, L.A. Rodriguez, N. Vollereaux, A.F. Yee, Nanopatterned polymer surfaces with bactericidal properties, Biointerphases 10 (2015) 021010.
[13] E.P. Ivanova, J. Hasan, H.K. Webb, G. Gervinskas, S. Juodkazis, V.K. Truong, A.H.F. Wu, R.N. Lamb, V.A. Baulin, G.S. Watson, J.A. Watson, D.E. Mainwaring, R.J. Crawford, Bactericidal activity of black silicon, Nature Communications 4 (2013) 2838.
[14] A. Kesel, R. Liedert, Learning from nature: Non-toxic biofouling control by shark skin effect, Comparative Biochemistry and Physiology, Part A: Molecular & Integrative Physiology 146 (2007) S130.
[15] C. Sengstock, M. Lopian, Y. Motemani, A. Borgmann, C. Khare, P.J.S. Buenconsejo, T.A. Schildhauer, A. Ludwig, M. Koller, Structure-related antibacterial activity of a titanium nanostructured surface fabricated by glancing angle sputter deposition, Nanotechnology 25 (2014) 195101.
[16] F. Ozel, H. Kockar, O. Karaagac, Growth of iron oxide nanoparticles by hydrothermal process: Effect of reaction parameters on the nanoparticle size, Journal of Superconductivity and Novel Magnetism 28 (2015) 823-829.
[17] A. Jaggessar, H. Shahali, A. Mathew, P.K.D.V. Yarlagadda, Bio-mimicking nano and micro-structured surface fabrication for antibacterial properties in medical implants, Journal of Nanobiotechnology 15 (2017) 64.
[18] M.D. Wang, C.C. Xing, K. Cao, L. Meng, J.B. Liu, Alignment-controlled hydrothermal growth of well-aligned ZnO nanorod arrays, Journal of Physics and Chemistry of Solids 75 (2014) 808-817.
[19] A. Jaggessar, A. Mathew, H. Wang, T. Tesfamichael, C. Yan, P.K.D.V. Yarlagadda, Mechanical, bactericidal and osteogenic behaviours of hydrothermally synthesised TiO2 nanowire arrays, Journal of the Mechanical Behavior of Biomedical Materials 80 (2018) 311-319.
[20] B. Liu, E.S. Aydil, Growth of Oriented Single-Crystalline Rutile TiO2 Nanorods on Transparent Conducting Substrates for Dye-Sensitized Solar Cells, Journal of the American Chemical Society 131 (2009) 3985-3990.
[21] T. Diu, N. Faruqui, T. Sjostrom, B. Lamarre, H.F. Jenkinson, B. Su, M.G. Ryadnov, Cicada-inspired cell-instructive nanopatterned arrays, Scientific Reports 4 (2014) 7122.
[22] Y.N. Xu, M.N. Liu, M.C. Wang, A. Oloyede, J.M. Bell, C. Yan, Nanoindentation study of the mechanical behavior of TiO2 nanotube arrays, Journal of Applied Physics 118 (2015).
[23] G. Collazzo, S. Jahn, N. Carreño, E. Foletto, Temperature and reaction time effects on the structural properties of titanium dioxide nanopowders obtained via the hydrothermal method, Brazilian Journal of Chemical Engineering 28 (2011) 265-272.
[24] A.C. Fischer-Cripps, Nanoindentation, 3rd;3;Third; ed., Springer Verlag, New York, NY, 2011.